Capacity fading mechanism of conversion-type FeF_3 electrode: investigation by electrochemical operando nuclear magnetic resonance spectroscopy

Keiji Shimoda[a,*], Masahiro Shikano[b], Miwa Murakami[a], Hikari Sakaebe[b]

[a] *Office of Society-Academia Collaboration for Innovation, Kyoto University, Uji, Kyoto 611-0011, Japan*

[b] *Research Institute of Electrochemical Energy, National Institute of Advanced Industrial Science and Technology* (*AIST*)*, Ikeda, Osaka 563-8577, Japan*

Abstract

FeF_3 has attracted considerable attention as a positive electrode material for next-generation rechargeable lithium ion batteries, because of its low cost, low risk, and high energy density, which facilitate a conversion-type lithiation/delithiation reaction. However, the conversion reaction of the FeF_3 electrode is known to suffer from capacity fading during repeated discharge–charge cycles. Herein, we find an interesting correlation between capacity fading behavior and spectral evolutions in electrochemical operando nuclear magnetic resonance (NMR) measurements. The operando ^7Li NMR spectra demonstrate the reversible formation of metallic Fe by the conversion process during the early discharge–charge cycles. However, it is gradually suppressed after repeated cycles. Moreover, LiF is augmented at the fully charged states, indicating that FeF_3 is no longer recovered after repeated cycles. The active material can converge into FeF_2 and LiF in the degraded electrode. Another factor associated with capacity degradation is the electrolyte decomposition occurring at high voltages, which results in a resistive film coating the electrode surface. We therefore conclude

that the film accumulation on repeated discharging inhibits the conversion reaction to metallic Fe and LiF, leading to a characteristic capacity fading behavior of FeF_3.

Keywords:

Rechargeable lithium ion batteries; capacity fading; FeF_3; operando NMR

*Corresponding author:

Keiji Shimoda

Office of Society-Academia Collaboration for Innovation, Kyoto University, Gokasho, Uji 611-0011, Japan

E-mail address: shimoda.keiji.6v@kyoto-u.ac.jp

Tel: +81-774-38-4967

Fax: +81-774-38-4996

1. Introduction

Rechargeable lithium ion batteries (LIBs) have been successfully employed worldwide as a power source for portable devices, and the global market for electric vehicles currently demands higher power, higher energy density, longer life, and lower cost batteries with a lower environmental impact. Significant effort has been dedicated to the development of improved battery materials. For example, conversion-type metal fluorides, such as CoF_2 and FeF_3, have been proposed as potential compounds for the development of next-generation LIB positive electrode materials because of their high theoretical capacities, which are significantly higher than those of topotactic intercalation-type materials, such as $LiCoO_2$ and $LiFePO_4$ [1].

FeF_3 comprises low-cost elements and has an excellent theoretical capacity of 712 mA h g^{-1}, assuming a three-electron charge transfer process ($FeF_3 + 3Li^+ + 3e^- \rightarrow Fe + 3LiF$). Arai et al. first reported the electrochemical performance of FeF_3 [2]. They showed a voltage plateau at ~3.0 V, and the discharging and charging capacities of 140 and 90 mA h g^{-1} were obtained at the first cycle with a voltage window between 2.0 and 4.5 V. X-ray diffraction (XRD) profiles for the disassembled electrode samples with compositions of $Li_{0.15}FeF_3$ and $Li_{0.5}FeF_3$ suggested that the lithiation reaction proceeded in a topotactic manner. Subsequently, Badway et al. prepared a FeF_3/C nanocomposite by ball milling to enhance electrochemical reactivity, which showed a significantly larger discharging capacity with a voltage window between 1.5 and 4.5 V [3]. Further, they showed a second voltage plateau at ~2.0 V and proposed the conversion reaction to metallic Fe and LiF [4].

Despite the merits mentioned above, practical applications of the FeF_3 electrode have been hindered by two factors. One is an unusually large voltage hysteresis between discharging and charging profiles, which results in low energy efficiency. The origin of the voltage hysteresis was recently investigated, and it was attributed to the reaction overpotential and different spatial evolutions of electrochemically active phases between discharging and charging processes [5]. The

second is the deterioration of cycle performance. The capacity fading behavior was observed after 10 cycles when a voltage window between 1.0 or 1.3 and 4.5 V was applied, which includes the conversion process [6]. Elucidation of the capacity fading mechanism of the FeF_3 electrode is vital to improve the reversibility of the electrode. A previous study using transmission electron microscopy (TEM) reported that metallic Fe and LiF were present in the FeF_3 nanowire electrode at the 50th-cycle charged state [7]. The formation of solid electrolyte interphase (passivation film) on the FeF_3 nanofiber surface was recognized after 50 cycles, which could increase the resistance of the electrode [8]. However, details of the capacity degradation process of FeF_3 were still not revealed. Recently, a comprehensive picture of the capacity fading mechanism of FeF_3 was provided using X-ray pair distribution function (PDF) analyses, X-ray absorption spectroscopy (XAS), X-ray photoelectron spectroscopy (XPS), and solid-state nuclear magnetic resonance (NMR) spectroscopy, and the incomplete oxidation to Fe^{3+} as well as aggregation of LiF at the charged state were shown [9].

In this brief report, an interesting correlation is shown between the capacity fading of FeF_3 and ^{7}Li spectral evolution in electrochemical operando NMR measurements, indicating the suppression of the formation of metallic Fe after repeated discharge–charge cycles. The spectral evolutions of LiF and surface film components are also examined in detail using high-resolution magic-angle spinning (MAS) NMR spectroscopy. A critical factor of the capacity fading mechanism is discussed.

2. Experimental

The procedure of electrode preparation and cell assembly is the same as that adopted in previous studies [9,10]. An active material composite was fabricated by mixing anhydrous FeF_3 powder (Rare Metallic) and acetylene black (AB, Denka) in a weight ratio of 70:25 using a planetary ball

mill (Premium line Pulverisette 7, Fritsch) at 200 rpm under an Ar atmosphere for 24 h. The electrode slurry was prepared by mixing the FeF_3/AB powder and polyvinylidene difluoride (PVDF, Kureha) under a dry air atmosphere to achieve a weight ratio of 95:5 with *N*-methyl-2-pyrrolidinone (NMP, Kishida Chemical), which was subsequently cast onto an Al foil current collector. The FeF_3 composite electrode sheet was obtained after drying at 90 °C under vacuum overnight.

CR2032 coin-type or laminate-type cells were assembled using Li foil as a counter electrode, polypropylene as a separator, and 1 M $LiPF_6$ in anhydrous ethylene carbonate (EC) and dimethyl carbonate (DMC) (1:1 vol. ratio) as an electrolyte solution (Tomiyama Pure Chemical Industries). The cells were galvanostatically cycled at room temperature between 1.0 and 4.5 V at a current density of 35.6 or 71.2 mA g^{-1} using a TOSCAT-3100 battery system (Toyo System). The coin cells were carefully disassembled at discharged or charged states in an Ar-filled glovebox for ex situ structural characterizations [9]. The electrode samples were washed with DMC and dried under vacuum.

NMR spectra were acquired on a DD2 600 spectrometer (Agilent Technologies) at a magnetic field of 14.1 T. Electrochemical operando ^{7}Li NMR measurements were performed with a homemade wide-bore static probe, in which the laminate cell was placed in the center of a 10 mm-diameter solenoid coil [11]. A Hahn echo pulse sequence was used with a first pulse width of 4.5 μs and a relaxation delay of 1 s. Each spectrum was averaged over 15 min. ^{7}Li, ^{19}F, and ^{31}P MAS NMR spectra were acquired with a wide-bore T3 MAS probe (Agilent Technologies). The samples were packed into 1.2 mmϕ MAS ZrO_2 rotors with airtight caps in the glovebox and spun at a spinning rate of 60 kHz (for ^{7}Li and ^{31}P) and 40 kHz (for ^{19}F to avoid signal overlapping) during the measurements. The MAS spectra were acquired using a rotor-synchronized Hahn echo

sequence with a π/2 pulse width of 1.0 μs and relaxation delays of 5 s (for ^{7}Li and ^{19}F) or 0.5 s (for ^{31}P). The signal intensities were normalized by sample weights in the rotors. Chemical shifts were referenced to 1 M LiCl solution at 0.0 ppm (for ^{7}Li), LiF at –203 ppm (for ^{19}F), and $(NH_4)H_2PO_4$ at 0.9 ppm (for ^{31}P).

3. Results and discussion

3.1. Spectral evolution of FeF_3 electrode and degradation during discharge–charge cycles

The discharge–charge profiles and capacity evolution of the FeF_3 electrode during 30 cycles are shown in Fig. 1. The initial discharging and charging capacities were 599 and 518 mA h g^{-1}, respectively, indicating a large capacity loss in the initial cycle. As for the discharging profiles, the intercalation-type lithiation reaction of FeF_3 to $Li_{\sim 1.0}FeF_3$ occurs above 2 V. Its detailed process and the structural models of the pertinent intermediate phases have been proposed [5,12,13]. Subsequently, the conversion reaction from $Li_{\sim 1.0}FeF_3$ to Fe + 3LiF is available below 2 V. Both the reactions seem to decrease in discharging capacity when the cycle proceeds up to 30 cycles. The observed capacity evolution was qualitatively similar to that in previous studies [6,9]. The discharging and charging capacities at a current density of 35.6 mA g^{-1} decreased rapidly compared with those at 71.2 mA g^{-1}, as shown in Fig. 1(b). The capacities gradually decreased from the ~5th cycle, and the decreasing rate was mitigated after ~15 cycles. The capacities at the 30th cycle were less than 100 mA h g^{-1}. These results suggest that the capacity fading proceeds more rapidly with larger initial capacities at smaller current densities because the conversion reaction accounting for 2/3 of the theoretical capacity is a key for capacity degradation as shown below. This is also consistent with a much smaller capacity fading with the discharge–charge cycles between 2.0 and 4.5 V [6].

Figure 2 shows operando ^{7}Li NMR spectra of a Li//FeF_3 cell during the initial discharge–charge

cycling. Two signals were observed in the lowermost spectrum before the electrochemical test. Sharp peaks at ~0 and ~276 ppm originated from the $LiPF_6$ salt in the electrolyte solution and metallic Li used as the counter electrode, respectively. A sequence of the spectra showed interesting features. In the intercalation reaction region, the spectra were almost unchanged, whereas it is considered that Li_xFeF_3 ($x \leq 1.0$) should form [14]. Subsequently, the peaks of the electrolyte solution and metallic Li split into two components at higher and lower frequencies during the conversion process. The degree of peak separation increased when the conversion proceeded. The peak splitting was interpreted as a consequence of the formation of metallic Fe in the conversion process, where the metallic Fe is nanosized (<~5 nm) and superparamagnetic in its magnetic nature [14,15]. A strong magnetic interaction from the Fe nanoparticles finely dispersed in the positive electrode can highly distort the ^{7}Li signals of the nearby LiF, electrolyte solution, and even metallic Li in the counter electrode. It should be emphasized that such an unusual spectral distortion by magnetic objects has never been reported to the best of the authors' knowledge. LiF shows a broad signal at ~0 ppm, if metallic Fe does not coexist. Therefore, the operando ^{7}Li NMR spectra indirectly confirm the formation of metallic Fe in the conversion region, and the degree of peak separation is correlated with the amount of metallic Fe. The spectral evolution was reversible, indicating that the metallic Fe disappeared during charging process.

Figure 3(a) shows operando ^{7}Li NMR spectra of the FeF_3 electrode at the fully discharged states up to 30 cycles. The degree of peak separation was significant and almost unchanged for the spectra up to the ~5th cycle (Fig. 3(b)). In contrast, it gradually decreased after that cycle. Finally, the distorted signals of LiF, electrolyte solution, and metallic Li converged into single sharp peaks at the 30th discharging. The spectral evolution of FeF_3 electrode was small in the 30th discharge–charge cycle (not shown). This indicates that metallic Fe hardly formed during the discharging

process at the 30th cycle. The evolution of the peak separation on discharging (Fig. 3(b)) was seemingly correlated with the evolution of capacity (Fig. 1(b)). These results strongly suggest that the capacity fading of FeF_3 observed is caused by suppression of the conversion reaction during the discharging process.

3.2. Spectral evolutions of LiF and surface film components during discharge–charge cycles

Figure 4(a) shows ^{7}Li MAS NMR spectra of the electrode samples disassembled at fully discharged and charged states for the 1st, 5th, 10th, 20th, and 30th cycles. The ^{7}Li signal of LiF was not observed in the spectrum of the 1st discharged sample, while the conversion of FeF_3 into metallic Fe was identified from X-ray PDF and XAS measurements [9]. In contrast, a small peak at –1.3 ppm with some spinning sidebands (SSBs) was shown in the subsequent charged sample. This signal can be attributed to LiF [16], and it disappeared in the discharging and increasingly reappeared in the charging up to the 10th cycle. LiF was identified both in the 20th and 30th discharged and charged samples. These results suggest that the ^{7}Li signal of LiF disappeared because of the strong magnetic interaction from the metallic Fe during the discharging process up to the 10th cycle, while LiF formed. Beyond the 10th cycle, metallic Fe did not form anymore during discharging, and the signal of LiF was observed. The 1st, 5th, and 10th discharged samples were attracted to magnets, but the 20th and 30th discharged and all the charged samples were not. LiF was confirmed in the 20th and 30th discharged samples, although the conversion reaction producing metallic Fe and LiF was suppressed. Furthermore, LiF increased when the cycle number of charging increased, clearly indicating that the recovery of FeF_3 was gradually suppressed, as in Fig. 4(b).

^{19}F MAS NMR spectra of the samples at fully discharged and charged states for the 1st, 5th, 10th, 20th, and 30th cycles are shown in Fig. 4(c). The signal of FeF_3 was not observed in the

pristine electrode, because F^- is directly bound to Fe^{3+} paramagnetic ions [14]. The ^{19}F signal of LiF was not observed in the spectrum of the 1st discharged sample, as shown for the ^7Li MAS spectrum, but the ^{19}F MAS spectrum showed a split spectral pattern similar to that observed in the operando ^7Li NMR spectra. This is an indication of Fe nanoparticles. In the subsequent charging, a small peak at –204 ppm with significant SSBs, which is attributable to LiF, was shown, as well as a peak of PVDF at –95 ppm [17]. These signals showed the split pattern in the discharging process up to the 10th cycle. The degree of splitting was decreased in the order of 1st, 5th, and 10th discharging, indicating again that the formation of metallic Fe was gradually suppressed. The signal of LiF was clearly observed both in discharging and charging beyond 10 cycles. Therefore, the operando ^7Li NMR and $^7Li/^{19}F$ MAS NMR measurements reveal that the capacity fading is associated with suppression of the formation of metallic Fe on discharging and/or suppression of the recovery of FeF_3 on charging. The intensity evolution of the LiF signal in the ^{19}F spectra resembles that in the ^7Li spectra, as shown in Figs. 4(b) and (d). This suggests that the loss of FeF_3 on charging is not correlated with the capacity fading observed after 10 cycles, because the amount of LiF increased linearly with charging up to the 20th cycle. In contrast, the loss of Fe nanoparticles on discharging is a key trigger of the capacity degradation, because they are correlated. Based on these observations and the average Fe valence state of ~2+ in the 30th discharged and charged states [9], it is considered that the active material finally converges into FeF_2 and LiF, not $LiFeF_3$, in the degraded electrode.

Figure 5(a) shows ^{31}P MAS NMR spectra of the samples disassembled at fully discharged and charged states for the 1st, 10th, 20th, and 30th cycles. Two signals were observed in the 1st charged sample: one comes from a phosphate species at –1.3 ppm and the other from $LiPF_6$ salt at –144 ppm [18]. These are phosphorus-containing inorganic film components formed on the electrode surface resulting from electrolyte decomposition during charging to high voltages [9]. The film

components detected up to the 20th cycle showed a reversible "breathing" behavior [20], that is a film growth process of precipitation at high voltages (charging) and dissolution at low voltages (discharging). The film components on the charged electrode increased up to the 10th cycle and almost constant after that (Fig. 5(b)). On the other hand, those on the discharged electrode increased after the 10th cycle, which is seemingly correlated with the observed capacity fading behavior of FeF_3. The surface film components on the electrode act as an impermeable layer for Li ions. This leads to a drastic increase in electrical resistance, as revealed using electrochemical impedance spectroscopy [9]. These results suggest that the accumulation of the resistive film inhibits the conversion reaction on discharging after the 10th cycle.

Our previous study found that the optimization of the electrolyte solvent from chain carbonates such as DMC and ethyl methyl carbonate (EMC) to cyclic carbonates such as EC and propylene carbonate (PC) suppressed the formation of surface film, resulting in the excellent improvement in the cycle performance of FeF_3 [9]. However, Fe^{2+} ions, instead of Fe^{3+}, were mainly observed in the 30th charged sample using the optimized electrolyte. Therefore, it would be necessary to control the particle size after repeated cycles for further improving the cycle performance. Anchoring the insulating FeF_3 nanoparticles on the graphene sheets provides an effective positive electrode with finely dispersed particles showing excellent rate performance and may control the size of the reaction products [20].

4. Conclusions

The capacity fading mechanism of the FeF_3 electrode was investigated by using the electrochemical operando NMR and high-resolution MAS NMR spectroscopy. The operando ^{7}Li NMR and ^{19}F MAS NMR spectra showed unusual spectral distortion behavior during the conversion process in the early discharge–charge cycles, suggesting the formation of metallic Fe nanoparticles. However,

the formation of metallic Fe was gradually suppressed during discharging after ~10 cycles. The ^{7}Li and ^{19}F MAS NMR spectra further indicated that LiF increased linearly on charging from the initial cycle, indicating that the recovery of FeF_3 was also suppressed. Therefore, the capacity fading mechanism of FeF_3 is attributed to the suppression of the conversion process to metallic Fe and LiF during discharging, with some contribution from the suppression of the recovery of FeF_3 during charging. Finally, the active material converged into FeF_2 and LiF in the degraded electrode. The electrolyte decomposition occurring at high voltages also provided an important contribution to the capacity degradation. Dynamic increase and decrease of resistive film components on charging and discharging were shown as a breathing behavior. The precipitation of film components at high voltages suppresses the recovery of FeF_3. In turn, its incomplete dissolution at low voltages leads to the film growth on repeated discharging, which inhibits the conversion reaction to metallic Fe and LiF, showing a characteristic capacity fading behavior. We concluded that the film accumulation on repeated discharging is a critical factor of a characteristic capacity fading of FeF_3. The present results emphasize that solid-state NMR techniques are a useful tool to characterize the degradation mechanism of electrode materials. The fundamental understandings achieved herein provide new insights for developing sophisticated conversion-type electrode materials to be utilized in next-generation LIBs.

Acknowledgments

This work was supported by the Research and Development Initiative for Scientific Innovation of New Generation Batteries 2 (RISING2) project, JPNP16001, from the New Energy and Industrial Technology Development Organization (NEDO), Japan. The authors would like to thank Mr. Takashi Moroishi for his support in sample preparation and electrochemical measurements.

References

[1] H. Li, P. Balaya, J. Maier, Li-storage via heterogeneous reaction in selected binary metal fluorides and oxides, J. Electrochem. Soc. 151 (2004) A1878–1885.

[2] H. Arai, S. Okada, Y. Sakurai, J. Yamaki, Cathode performance and voltage estimation of metal trihalides, J. Power Sources 68 (1997) 715–719.

[3] F. Badway, N. Pereira, F. Cosandey, G.G. Amatucci, Carbon-metal fluoride nanocomposites: Structure and electrochemistry of FeF_3 : C, J. Electrochem. Soc. 150 (2003) A1209–1218.

[4] F. Badway, F. Cosandey, N. Pereira, G.G. Amatucci, Carbon metal fluoride nanocomposites: High-capacity reversible metal fluoride conversion materials as rechargeable positive electrodes for Li batteries, J. Electrochem. Soc. 150 (2003) A1209–1218.

[5] L. Li, R. Jacobs, P. Gao, L. Gan, F. Wang, D. Morgan, S. Jin, Origins of large voltage hysteresis in high-energy-density metal fluoride lithium-ion battery conversion electrodes, J. Am. Chem. Soc. 138 (2016) 2838–2848.

[6] A. Kitajou, I. Tanaka, Y. Tanaka, E. Kobayashi, H. Setoyama, T. Okajima, S. Okada, Discharge and charge reaction of perovskite-type MF_3 (M = Fe and Ti) cathodes for lithium-ion batteries, Electrochemistry 85 (2017) 472–477.

[7] L. Li, F. Meng, S. Jin, High-capacity lithium-ion battery conversion cathodes based on iron fluoride nanowires and insights into the conversion mechanism, Nano Lett. 12 (2012) 6030–6037.

[8] W. Fu, E. Zhao, Z. Sun, X. Ren, A. Magasinski, G. Yushin, Iron fluoride-carbon nanocomposite nanofibers as free-standing cathodes for high-energy lithium batteries, Adv. Funct. Mater. 28 (2018) 1801711.

[9] H. Senoh, K. Matsui, M. Shikano, T. Okumura, H. Kiuchi, K. Shimoda, K. Yamanaka, T. Ohta, T. Fukunaga, H. Sakaebe, E. Matsubara, Degradation mechanism of conversion-type iron

trifluoride: Toward improvement of cycle performance, ACS Appl. Mater. Interfaces 11 (2019) 30959–30967.

[10] K. Kumagae, K. Okazaki, K. Matsui, H. Horino, T. Hirai, J. Yamaki, Z. Ogumi, Improvement of cycling performance of FeF_3-based lithium-ion battery by boron-based additives, J. Electrochem. Soc. 163 (2016) A1633–1636.

[11] K. Shimoda, M. Murakami, D. Takamatsu, H. Arai, Y. Uchimoto, Z. Ogumi, *In situ* NMR observation of the lithium extraction/insertion from $LiCoO_2$ cathode, Electrochim. Acta 108 (2013) 343–349.

[12] R.E. Doe, K.A. Persson, Y.S. Meng, G. Ceder, First-principles investigation of the Li-Fe-F phase diagram and equilibrium and nonequilibrium conversion reactions of iron fluorides with lithium, Chem. Mater. 20 (2008) 5274–5283.

[13] W. Zhang, P.N. Duchesne, Z.-L. Gong, S.-Q. Wu, L. Ma, Z. Jiang, S. Zhang, P. Zhang, J.-X. Mi, Y. Yang, In situ electrochemical XAFS studies on an iron fluoride high-capacity cathode material for rechargeable lithium batteries, J. Phys. Chem. C 117 (2013) 11498–11505.

[14] N. Yamakawa, M. Jiang, B. Key, C.P. Grey, Identifying the local structures formed during lithiation of the conversion material, iron fluoride, in a Li ion battery: A solid-state NMR, X-ray diffraction, and pair distribution function analysis study, J. Am. Chem. Soc. 131 (2009) 10525–10536.

[15] T. Takami, K. Matsui, H. Senoh, N. Taguchi, M. Shikano, H. Sakaebe, T. Fukunaga, Magnetic behavior of Fe nanoparticles driven by phase transition of FeF_3, J. Alloys Compd. 769 (2018) 539–544.

[16] M. Murakami, H. Yamashige, H. Arai, Y. Uchimoto, Z. Ogumi, Direct evidence of LiF formation at electrode/electrolyte interface by ^{7}Li and ^{19}F double-resonance solid-state NMR spectroscopy, Electrochem. Solid-State Lett. 14 (2011) A134–137.

[17] M. Murakami, H. Yamashige, H. Arai, Y. Uchimoto, Z. Ogumi, Association of paramagnetic species with formation of LiF at the surface of $LiCoO_2$, Electrochim. Acta 78 (2012) 49–54.

[18] A.V. Plakhotnyk, L. Ernst, R. Schmutzler, Hydrolysis in the system $LiPF_6$–propylene carbonate–dimethyl carbonate–H_2O, J. Fluor. Chem. 126 (2005) 27–31.

[19] M. Cuisinier, N. Dupré, J.-F. Martin, R. Kanno, D. Guyomard, Evolution of the $LiFePO_4$ positive electrode interface along cycling monitored by MAS NMR, J. Power Sources 224 (2013) 50–58.

[20] J. Liu, Y. Wan, W. Liu, Z. Ma, S. Ji, J. Wang, Y. Zhou, P. Hodgson, Y. Li, Mild and cost-effective synthesis of iron fluoride-graphene nanocomposites for high-rate Li-ion battery cathodes, J. Mater. Chem. A 1 (2013) 1969–1975.

Figures and Figure captions

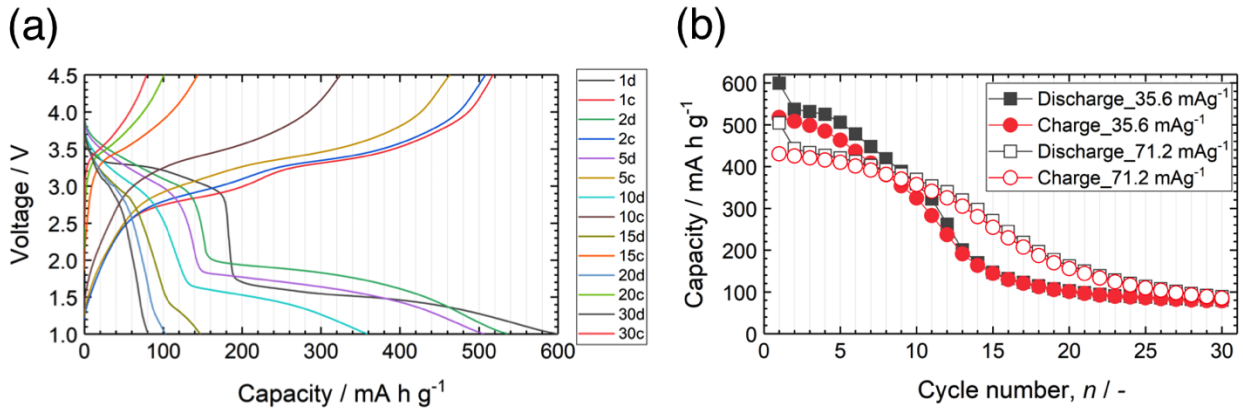

Fig. 1. (a) Discharge–charge profiles and (b) capacity evolution of the FeF_3 electrode during 30 cycles. The cell was galvanostatically cycled at room temperature between 1.0 and 4.5 V at a current density of 35.6 mA g^{-1} (Data at 71.2 mA g^{-1} are also shown in (b) for comparison). The *n*d and *n*c indicate *n*th cycle discharging and charging, respectively.

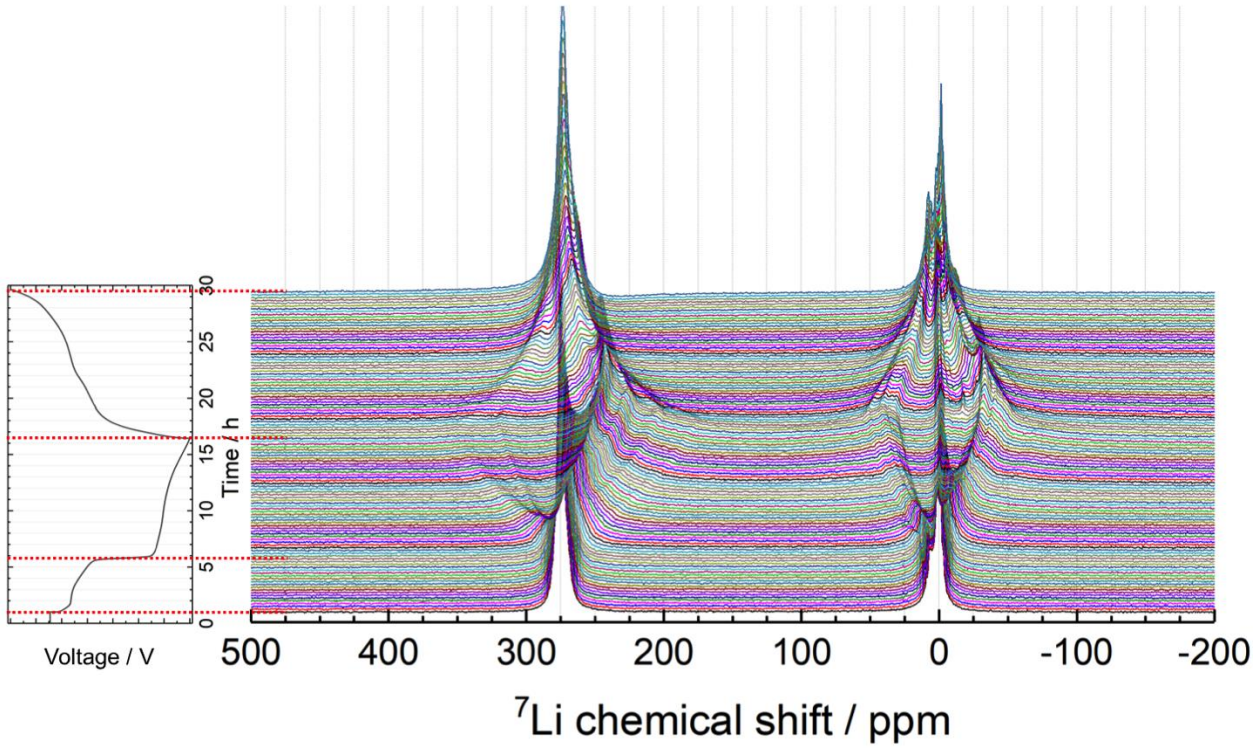

Fig. 2. Operando ^{7}Li NMR spectra of the FeF_3 electrode during the initial cycle. The cell was cycled between 1.0 and 4.5 V at a current density of 35.6 mA g^{-1}.

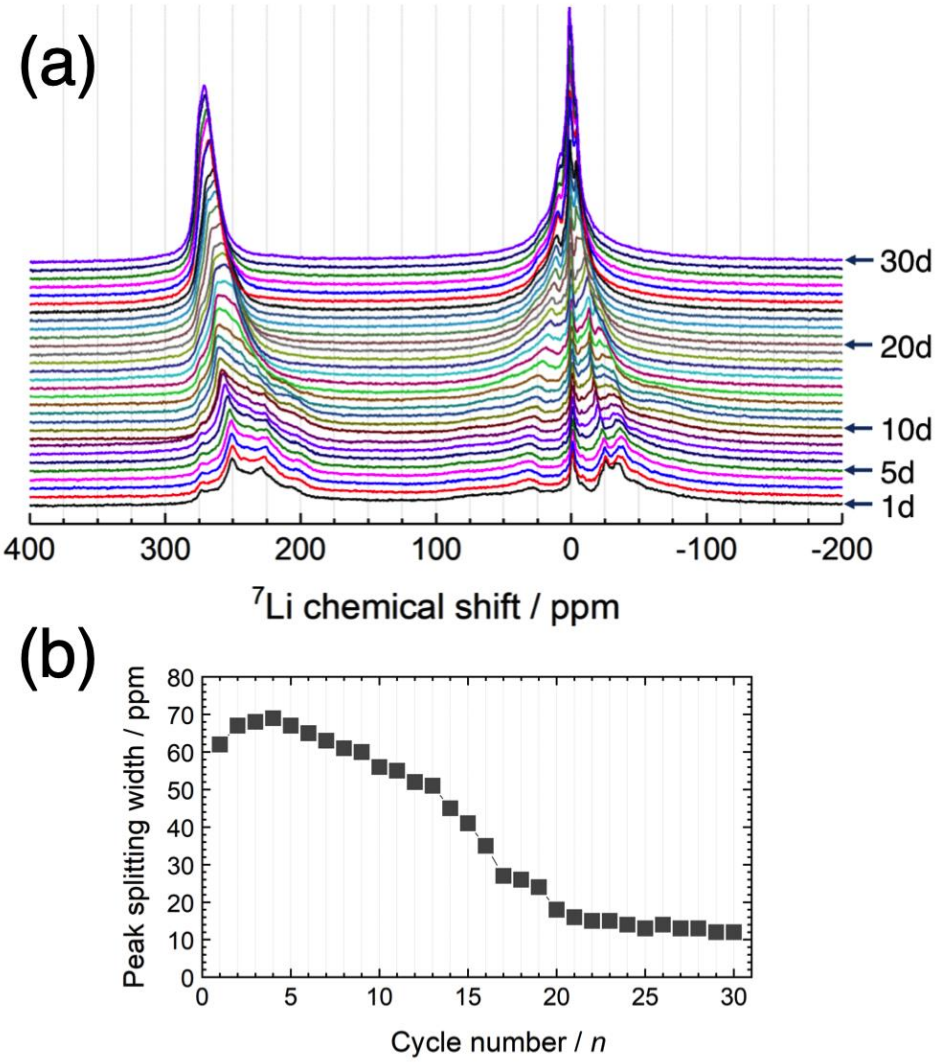

Fig. 3. (a) Operando ^{7}Li NMR spectra of the FeF_3 electrode at the fully charged states during 30 cycles. The cell was cycled at a current density of 71.2 mA g^{-1}. (b) Evolution of the splitting width between the peaks at –35 and 30 ppm in the lowermost spectrum in (a).

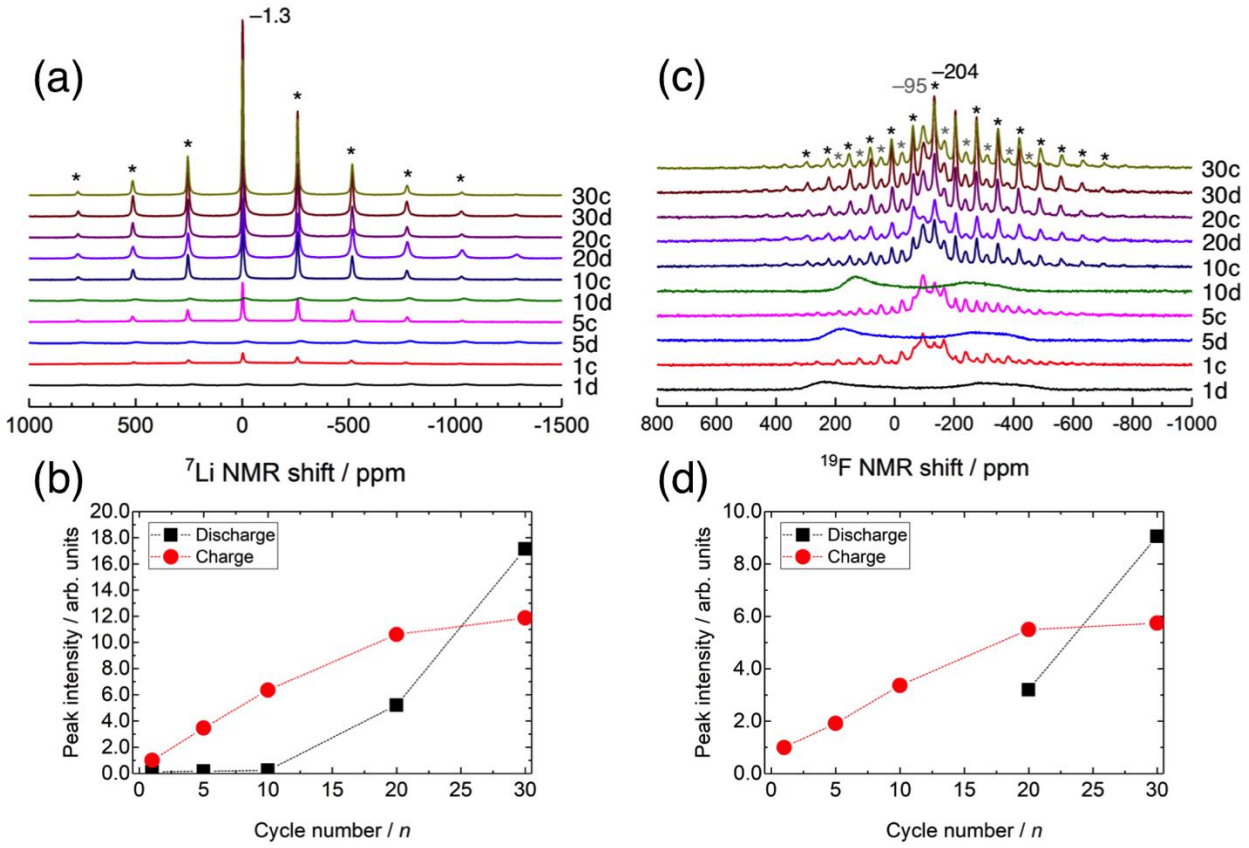

Fig. 4. (a) ^{7}Li MAS NMR spectra of the FeF_3 electrode during discharge–charge cycles and (b) normalized ^{7}Li intensity evolution of LiF signal at –1.3 ppm, and (c) ^{19}F MAS NMR spectra and (d) normalized ^{19}F intensity evolution of LiF signal at –204 ppm. Asterisks indicate SSBs.

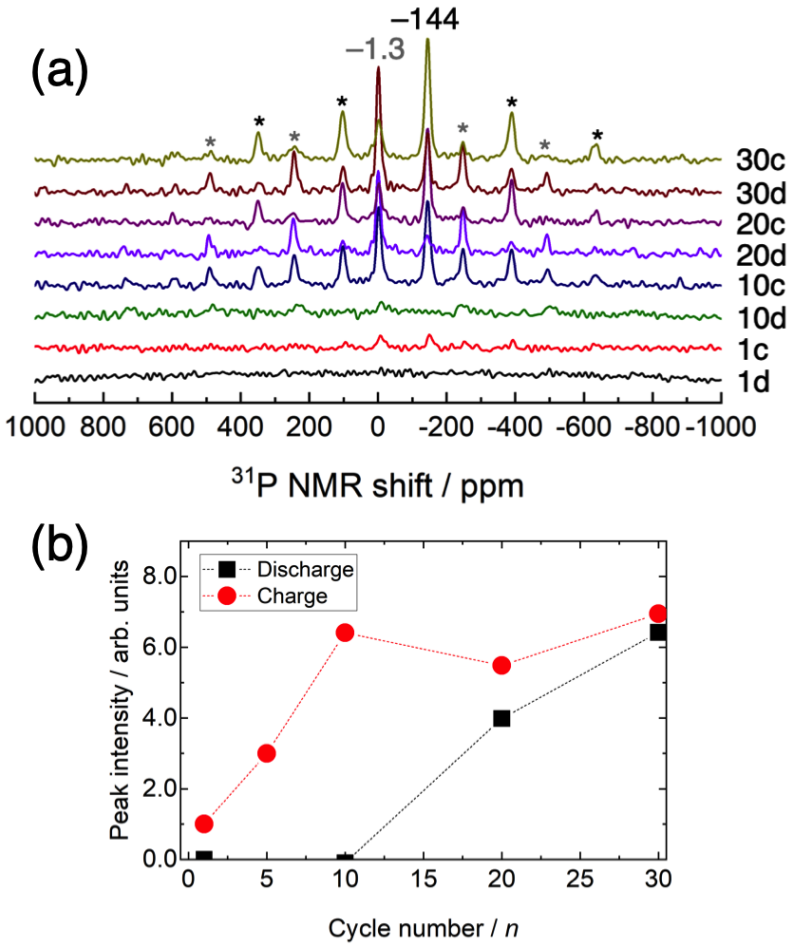

Fig. 5. (a) ^{31}P MAS NMR spectra of the FeF_3 electrode during discharge–charge cycles and (b) normalized ^{31}P intensity evolution of summed signals at –1.3 and –144 ppm (a point for 5c is added). Asterisks indicate SSBs.